

Surface Functionalization of Single Superparamagnetic Iron Oxide Nanoparticles for Targeted Magnetic Resonance Imaging

Esther Amstad, Stefan Zurcher, Alireza Mashaghi, Joyce Y. Wong, Marcus Textor, and Erik Reimhult*

Magnetic resonance imaging (MRI), a non-invasive, non-radiative technique, is thought to lead to cellular or even molecular resolution if optimized targeted MR contrast agents are introduced. This would allow diagnosing progressive diseases in early stages. Here, it is shown that the high binding affinity of poly(ethylene glycol)-gallol (PEG-gallol) allows freeze drying and re-dispersion of 9 ± 2 -nm iron oxide cores individually stabilized with ≈ 9 -nm-thick stealth coatings, yielding particle stability for at least 20 months. Particle size, stability, and magnetic properties of PEGylated particles are compared to Feridex, a commercially available untargeted negative MR contrast agent. Biotin-PEG(3400)-gallol/methoxy-PEG(550)-gallol stabilized nanoparticles are further functionalized with biotinylated human anti-VCAM-1 antibodies using the biotin–neutravidin linkage. Binding kinetics and excellent specificity of these nanoparticles are demonstrated using quartz crystal microbalance with dissipation monitoring (QCM-D). These MR contrast agents can be functionalized with any biotinylated ligand at controlled ligand surface density, rendering them a versatile research tool.

Keywords:

- functionalization
- MRI
- contrast agents
- stabilization
- targeting

1. Introduction

The good biocompatibility and low cost of iron oxide nanoparticles render them suitable for many biomedical applications^[1,2] such as cell separation, ferrying cells, and

contrast-enhanced MRI.^[3] Much work has been dedicated to the synthesis of iron oxide nanoparticles because the synthesis determines particle composition, size distribution, and morphology.^[4,5] These are parameters directly influencing physical properties^[6,7] as well as clearance rate and clearance route of nanoparticles.^[8,9]

Several complementary non-invasive techniques for biomedical imaging, for example, MRI, single-photon emission tomography (SPECT), positron emission tomography (PET), and computed tomography (CT), are used to elucidate the evolution and progression of many different diseases in humans and animals. One important advantage of MRI over SPECT, PET, and CT is its non-radiating nature. Moreover, MRI allows for imaging soft tissues in contrast to PET and SPECT, and it does so with higher contrast resolution than CT. The inherent low sensitivity of MRI compared to SPECT and PET can be improved by introducing MR contrast agents

[*] Dr. E. Reimhult, E. Amstad, Dr. S. Zurcher, A. Mashaghi, Prof. Dr. M. Textor
Laboratory for Surface Science and Technology
ETH Zurich, 8093 Zurich (Switzerland)
E-mail: erik.reimhult@mat.ethz.ch
Dr. J. Y. Wong
Department of Biomedical Engineering
Boston University, MA 02215 (USA)

Supporting Information is available on the WWW under <http://www.small-journal.com> or from the author.

DOI: 10.1002/smll.200801328

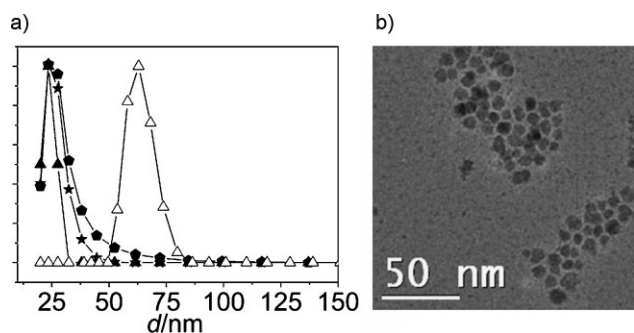


Figure 2. a) Number-weighted DLS measurement of mPEG(550)-gallol/biotin-PEG(3400)-gallol stabilized nanoparticles kept as powder for 20 months before re-dispersion in HEPES (-▲-), mPEG(550)-gallol/biotin-PEG(3400)-gallol stabilized nanoparticles 20 months after stabilization in HEPES (-●-), mPEG(550)-gallol/biotin-PEG(3400)-gallol stabilized nanoparticles stored as powder for 1 year, re-dispersed in PBS for 1 year (-★-) and Feridex (-△-). b) TEM image showing mPEG(550)-gallol/biotin-PEG(3400)-gallol stabilized nanoparticles dried onto an 8-nm-thick carbon film. The nanoparticles are well separated by the PEG shell.

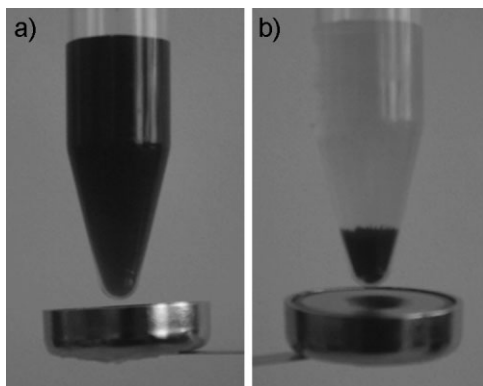


Figure 3. a) The biotin-PEG(3400)-gallol/mPEG(550)-gallol dispersant layer surrounding the iron oxide nanoparticle cores is stable and thick enough to prevent particle agglomeration in the presence of a small external magnet, even after particles have been dispersed in PBS for more than 1 year. b) In the absence of the dispersant layer, iron oxide cores agglomerate and thus sediment instantaneously upon approaching a small external magnet. (See also videos in the Supporting Information.)

individual iron oxide cores is too small to overcome Brownian motion and thus to cause sedimentation, the magnetic moment of agglomerates is high enough to be strongly attracted by the weak external magnet, which results in instantaneous sedimentation.

The single-domain core of individually PEG-gallol stabilized iron oxide nanoparticles had a diameter of 9 ± 2 nm, as determined by transmission electron microscopy (TEM; Figure 4). High-resolution TEM (HRTEM) micrographs of single-domain iron oxide nanoparticles oriented in the (221) direction revealed an Fe–Fe distance of 3.0 ± 0.3 Å (Figure 4a) in good agreement with what has been previously reported for magnetite^[32] and maghemite.^[33] The BET surface area of uncoated powder was $88 \text{ m}^2 \text{ g}^{-1}$. This area was lower than expected for the average particle diameter of 9 nm; however,

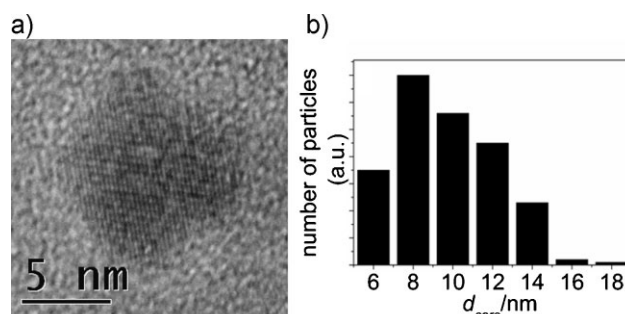


Figure 4. a) HRTEM of mPEG(550)-gallol stabilized iron oxide nanoparticles show that particles are single domain with an Fe–Fe distance of 3.0 ± 0.3 Å in the (221) direction. b) Analysis of TEM micrographs revealed an iron oxide core size of 9 ± 2 nm (measured on 240 particles).

during centrifugation of freeze-dried and re-dispersed particles, larger particles were removed and thus excluded from the core size evaluations of re-dispersed particles performed by TEM.

Thermogravimetric analysis coupled to a Fourier transform infrared spectrometer (TGA-FTIR) was performed to validate the presence and quantify the amount of PEG-gallol on the nanoparticle surface. The weight loss measured between 200 and 400 °C during TG analysis could be clearly assigned to the decomposition of PEG by FTIR spectroscopy, proving that PEG-gallol was adsorbed on the nanoparticles. The weight loss between 200 and 400 °C measured by TG analysis for mPEG(550)-gallol, mPEG(550)-gallol/biotin-PEG(3400)-gallol, and mPEG(5000)-gallol stabilized nanoparticles was 11, 15, and 50 wt%, respectively. Based on these values, approximately 235 molecules were adsorbed per particle ($194 - 198 \mu\text{mol} \cdot \text{g}_{\text{iron-oxide}}^{-1}$). This corresponds to an average contact area of $74 - 76 \text{ Å}^2$ per molecule for all dispersants, independent of PEG molecular weight. For mPEG(5000)-stabilized particles, the corresponding PEG density is $1.3 \text{ PEG}(5000) \text{ molecules nm}^{-2}$, which is more than three times higher than the maximum PEG(5000) density reported ($0.4 \text{ PEG}(5000) \text{ nm}^{-2}$) for mPEG(5000)-DOPA₃ adsorbed onto flat TiO₂ surfaces.^[34] The molar ratio of biotin-PEG(3400)-gallol to mPEG(550)-gallol could thus be calculated by comparing the difference in mass loss measured with TGA between mPEG(550)-gallol and mPEG(550)-gallol/biotin-PEG(3400)-gallol stabilized particles assuming that the dispersant packing is independent on the PEG molecular weight. Based on these calculations, the dispersant shell surrounding the iron oxide consisted of 9 mol% biotin-PEG(3400)-gallol and 91 mol% mPEG(550)-gallol. The iron oxide cores had been stabilized by adding 10 mol% biotin-PEG(3400)-gallol and 90% mPEG(550)-gallol to the uncoated nanoparticle suspension, which is close to the percentage of these dispersants adsorbed on the particles. Assuming particles were perfectly spherical and had a core diameter of 9 nm this equaled 20 biotin sites per particle.

Zeta potential measurements revealed a point of zero charge (PZC) of 6.7 for uncoated iron oxide nanoparticles, in good agreement with what other groups have reported.^[35–37] The isoelectric point (IEP) of nanoparticles stabilized with

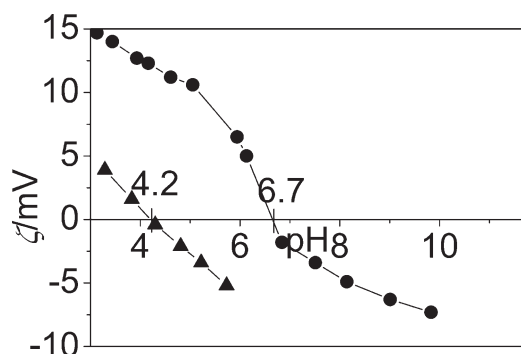


Figure 5. Zeta potential measurements revealed a PZC of uncoated iron oxide nanoparticles (●) of 6.7. Stabilization of these nanoparticles with mPEG(550)-gallol (▲) shifted the IEP to 4.2.

mPEG(550)-gallol and dialyzed for 24 h against Millipore water, was shifted to 4.2 (Figure 5). The difference between the PZC of unstabilized and the IEP of mPEG(550)-gallol stabilized nanoparticles was assumed to result from the adsorption of gallol, as was reported by Studart et al. for Al_2O_3 nanoparticles.^[38] The protons from gallol likely dissociated prior to binding to iron oxide introducing negative charges to the surface and thus shifting the IEP toward more acidic values.

2.2. Magnetic Properties

The superparamagnetic properties of these single-domain iron oxide nanoparticles were confirmed with superconducting quantum interference device (SQUID) measurements (Figure 6a). The room-temperature saturation magnetizations of unstabilized and mPEG(550)-gallol stabilized particles was 58 and 50 $\text{emu} \cdot \text{g}_{\text{Fe}}^{-1}$, respectively, which were within the ranges of reported values.^[39,40] A reduction of the saturation magnetization upon iron oxide nanoparticle stabilization with different dispersants has also been described by other groups.^[41,42] Based on the observed decrease, the magnetization of the top $\approx 2 \text{ \AA}$ is likely to have been lost.^[41]

R_2 and the ratio R_2/R_1 are parameters for contrast enhancement of conventional T_2 -weighted MR images typically measured when negative contrast agents such as iron oxide nanoparticles are used. R_2 of iron oxide nanoparticles stabilized with mPEG(550)-gallol and biotin-PEG(3400)-gallol was higher ($134 \pm 91 \text{ mmol}_{\text{Fe}}^{-1} \cdot \text{S}^{-1}$) than R_2 of Feridex ($102 \pm 51 \text{ mmol}_{\text{Fe}}^{-1} \cdot \text{S}^{-1}$), measured at $T = 39^\circ\text{C}$ and $B_0 = 11.7 \text{ T}$. Furthermore, R_1 was substantially lower for the former ($1.4 \pm 0.21 \text{ mmol}_{\text{Fe}}^{-1} \cdot \text{S}^{-1}$) compared to R_1 for Feridex ($2.7 \pm 0.21 \text{ mmol}_{\text{Fe}}^{-1} \cdot \text{S}^{-1}$) (Figure 6b and c) resulting in a more than two times higher R_2/R_1 ratio of PEG-gallol stabilized particles compared to Feridex.

2.3. Nanoparticle Functionalization

Neutravidin was bound to biotin-PEG(3400)-gallol/mPEG(550)-gallol stabilized particles (Figure 7). The number of neutravidins adsorbed per particle was maximized to prevent aggregation of different particles, which can bind to the same neutravidin since neutravidin has four biotin binding

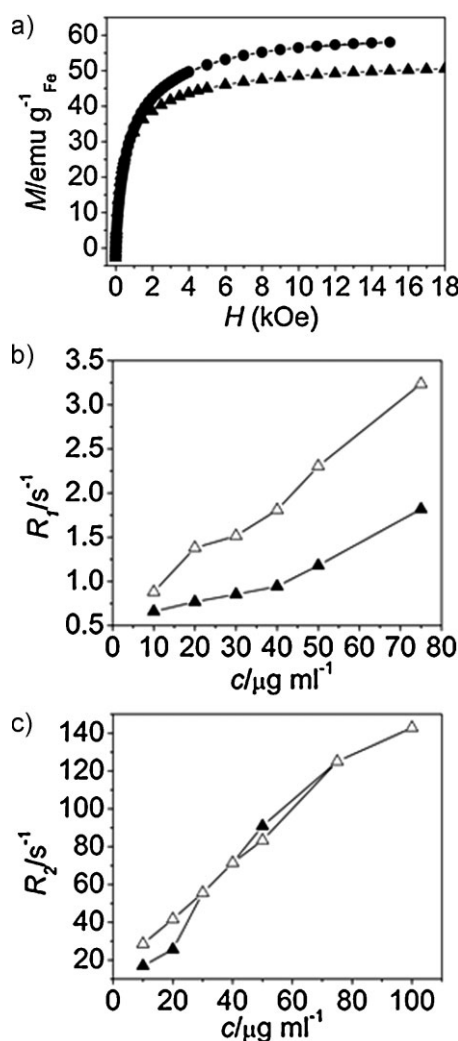


Figure 6. a) Uncoated iron oxide nanoparticles (●) had an M_s of 58 $\text{emu} \cdot \text{g}_{\text{Fe}}^{-1}$ as measured with SQUID assuming iron oxide consisted exclusively of Fe_3O_4 . Stabilization of these nanoparticles with mPEG(550)-gallol (▲) decreased M_s to 50 $\text{emu} \cdot \text{g}_{\text{Fe}}^{-1}$. A comparison of b) R_1 and c) R_2 of mPEG(550)-gallol stabilized nanoparticles (▲) and Feridex (△) as a function of particle concentration at 39°C and $B_0 = 11.7 \text{ T}$ showed that while Feridex had a higher R_1 value of $2.7 \pm 0.21 \text{ mmol}_{\text{Fe}}^{-1} \cdot \text{S}^{-1}$ compared to mPEG-gallol stabilized particles with $1.4 \pm 0.2 \text{ mmol}_{\text{Fe}}^{-1} \cdot \text{S}^{-1}$, mPEG-gallol stabilized particles had a higher R_2 value with $134 \pm 91 \text{ mmol}_{\text{Fe}}^{-1} \cdot \text{S}^{-1}$ compared to Feridex ($102 \pm 51 \text{ mmol}_{\text{Fe}}^{-1} \cdot \text{S}^{-1}$).

sites. The neutravidin saturation concentration of these biotinylated particles was determined with a) DLS (Figure 8a), b) fluorescence-activated cell sorting (FACS; Figure 8b), and c) QCM-D (Figure 8c) by adding different amounts of neutravidin to PBS containing 1 $\text{mg} \cdot \text{mL}^{-1}$ biotin-PEG(3400)-gallol/mPEG(550)-gallol stabilized iron oxide nanoparticles. The hydrodynamic diameter of neutravidin-coated particles increased with increasing neutravidin concentration up to a protein concentration of 7 $\mu\text{mol} \cdot \text{mL}^{-1}$ yielding an increase in hydrodynamic diameter of 12 nm (Figure 8a). Streptavidin, another avidin derivative of similar molecular weight as neutravidin,^[27] has a thickness of $\approx 5 \text{ nm}$.^[43] The observed

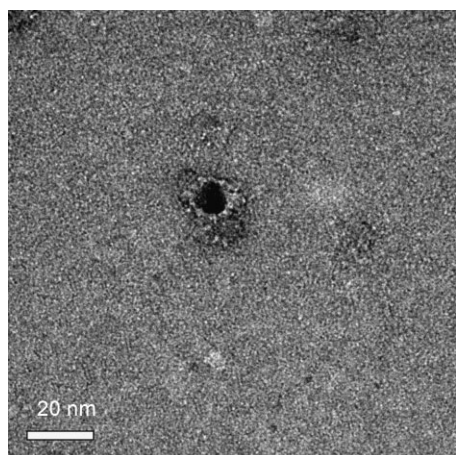


Figure 7. Negatively stained TEM image of a single, mPEG(550)-gallol/biotin-PEG(3400)-gallol-stabilized Fe_3O_4 particle further functionalized with a saturated neutravidin layer (white shapes surrounding particle).

increase in hydrodynamic diameter of close to twice the neutravidin thickness thus agrees well with particles surrounded by a neutravidin monolayer. The increased fluorescence signal of nanoparticles with increasing addition of FITC-labeled neutravidin up to a concentration of $7 \mu\text{mol g}_{\text{iron oxide}}^{-1}$ further supported the findings from DLS (Figure 8b). Lastly, SiO_2 -coated QCM-D sensors were used to form a neutravidin monolayer on top of a non-fouling supported lipid bilayer (SLB) containing biotinylated lipids. Particle binding to the neutravidin monolayer decreased as the surface coverage of neutravidin on the particles increased. No binding was observed at $7 \mu\text{mol g}_{\text{iron oxide}}^{-1}$ (Figure 8c), which corresponds to eight neutravidin molecules per particle assuming an iron oxide density of 5.18 g cm^{-3} . If one considers that at least two biotin binding sites per neutravidin are accessible this would correspond to close to full saturation of the average 20 biotin binding sites per particle estimated from our TGA-FTIR results. Based on these results, it is unlikely that any free biotin site was still accessible after saturating the particle shell with neutravidin. This was supported by the observed plateau in both the DLS and FACS curves, indicating that there was no particle aggregation.

Real-time binding kinetics and binding specificity of functionalized particles were investigated using QCM-D. Recombinant human VCAM-1 chimera was immobilized via protein A onto SiO_2 QCM-D sensor crystals (schematically shown in Figure 9a). Neutravidin pre-coated nanoparticles were further functionalized with biotinylated human anti-VCAM-1 antibodies. Upon exposure of such functionalized nanoparticles to the sensor, fast, and specific binding was observed. Only minimal frequency and dissipation shifts (-1.5 Hz and 1.2×10^{-6} , respectively) were measured 2 h after particle injection for particles lacking the anti-VCAM-1 antibody. Corresponding shifts of -30 Hz and 18.7×10^{-6} for particles functionalized with biotinylated human anti-VCAM-1 antibody demonstrated that the binding was specific (Figure 9b). Neither neutravidin pre-coated particles bearing biotinylated anti-E-selectin antibodies nor PEGylated iron oxide particles or bovine serum albumin (BSA) adsorbed

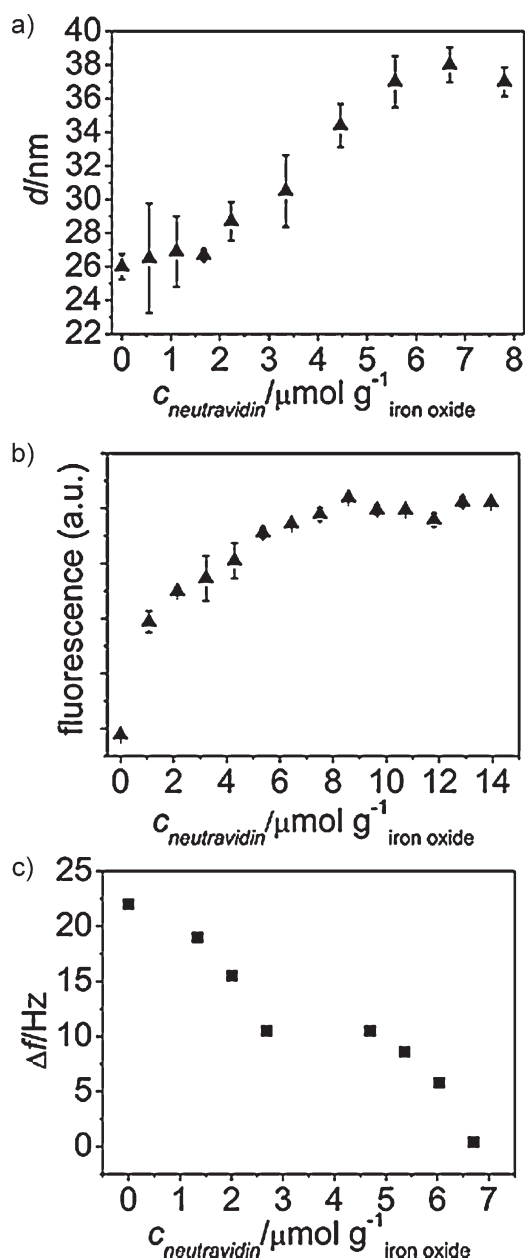


Figure 8. The neutravidin saturation concentration of biotin-PEG(3400)-gallol/mPEG(550)-gallol-stabilized iron oxide nanoparticles was determined by a) DLS where an increase in hydrodynamic diameter of particles bearing increasing amounts of neutravidin was measured up to the neutravidin saturation concentration, b) FACS measurements revealing an increase in fluorescence of particles coated with increasing amounts of FITC-labeled neutravidin up to the neutravidin saturation concentration, and c) QCM-D measurements demonstrating particle binding toward a neutravidin monolayer. Binding decreased to 0 with increasing amount of neutravidin bound to the biotinylated particles. The neutravidin monolayer was immobilized onto SiO_2 -coated sensors through non-fouling SLBs containing biotinylated lipids. All three techniques showed that maximally $\approx 7 \mu\text{mol g}_{\text{iron oxide}}^{-1}$ can be bound to the biotin-bearing nanoparticles, corresponding to eight neutravidin molecules per particle.

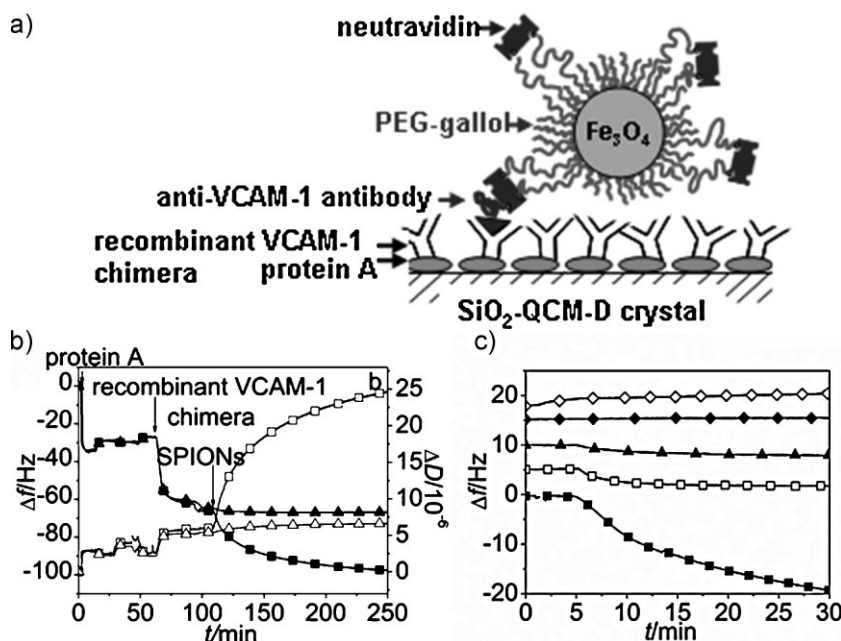


Figure 9. a) Schematic of the immobilization of recombinant human VCAM-1 chimera onto SiO₂ QCM-D crystals via protein A and the layer-by-layer build-up of functionalized Fe₃O₄ nanoparticles. These nanoparticles were stabilized with a mixture of mPEG(550)-gallol and biotin-PEG(3400)-gallol, further coated with 7 μmol neutravidin g_{iron oxide}⁻¹ and subsequently functionalized with 1.4 μmol neutravidin g_{iron oxide}⁻¹ biotinylated anti-human VCAM-1 antibodies. b) Whereas non-specific binding of neutravidin-coated nanoparticles (SPIONs) lacking anti-VCAM antibodies was negligible as shown in QCM-D experiments by small changes in frequency (▲) and dissipation (△), there was strong and fast binding of SPIONs functionalized with anti-VCAM-1 antibodies to recombinant VCAM-1 chimeras, indicated by a large frequency (■) and dissipation (□) shift after 2 h exposure. c) Binding of PEG-gallol stabilized neutravidin-coated particles bearing no antibodies (▲) and particles functionalized with human E-selectin antibodies (△) to VCAM-1 chimeras was considerably lower compared to anti-VCAM-1 antibodies functionalized particles (■). No significant binding of anti-VCAM-1 antibody functionalized particles toward E-cadherins which had previously been immobilized through protein A on SiO₂-coated QCM-D crystals (◆) or human serum immobilized on Au-coated QCM-D crystals (◇) prior to particle injection was measured. Taken together, these experiments demonstrated high binding specificity of anti-VCAM-1 antibody functionalized particles.

significantly on surfaces presenting recombinant human VCAM-1 chimeras. Specificity of the observed binding interaction was demonstrated in that particles functionalized with anti-VCAM-1 antibodies did not bind to cadherins nor to human serum (Figure 9c and S1 in Supporting Information). However, binding of functionalized particles was highly dependent on the amount of anti-VCAM-1 antibodies added to neutravidin precoated nanoparticles (see Figure S2 in Supporting Information). Further control experiments of the binding of biotinylated anti-VCAM-1 antibodies with and without neutravidin to recombinant VCAM-1 chimera and binding of functionalized particles toward protein A are also given in the Supporting Information (Figure S1).

3. Discussion

The high binding affinity of PEG-gallol toward iron oxide allowed freeze-drying and re-dispersion of individually

stabilized iron oxide nanoparticles and led to one of the highest reported particle stabilities under physiological conditions to date. Long-term stability of magnetite nanoparticles stabilized with polyol molecules^[44] and Fe/Fe_xO_y core/shell particles stabilized with PEG-dopamine^[21] have been reported during the preparation of this work. However, none of these particles were further functionalized and specific targeting capability demonstrated, nor were they characterized and tested as MRI contrast agents. We also demonstrate the additional possibility to freeze-dry and re-disperse individually PEG-gallol stabilized iron oxide nanoparticles. This simplifies particle handling and allows for long-term particle storage, which is of high commercial value. In contrast to what Carpenter and co-workers^[45] and Xie et al.^[18] have reported for core/shell Fe/Fe₂O₃ and Fe₃O₄ nanoparticles stabilized with PEG(600)-dopamine and PEG(2000)-trichloro-s-triazine-dopamine, respectively, no degradation or corrosion of iron oxide nanoparticles upon stabilization was observed with PEG-gallol.

The much lower standard deviation of the hydrodynamic diameter of mPEG-gallol-stabilized nanoparticles compared to Feridex (7% versus 33%) is a result of the high binding affinity of gallol and trihydroxy-benzene, which leads to a well-defined surface chemistry and no aggregation. The weight percent of dispersants adsorbed on nanoparticles related to the BET surface area results in a dispersant contact area of 75 Å². This corresponds to a dispersant packing density of 30% if one refers to the reported

theoretical cross-sectional anchor group area perpendicular to the benzyl ring of 22.3 Å².^[46] The PEG layer of iron oxide nanoparticles stabilized with biotin-PEG(3400)-gallol/mPEG(550)-gallol is approximately 9 nm thick, if the iron oxide core diameter determined by TEM is compared to the hydrodynamic diameter measured with DLS and XDC. With a single iron oxide core per particle and a stable, dense dispersant coating defined only by the gallol anchor, the particle size distribution is determined solely by the size distribution of the core and the choice of PEG molecular weight.

4. Conclusions

We have shown that a layer-by-layer build-up of successive shells of superparamagnetic iron oxide nanoparticles individually stabilized with a mixture of mPEG(550)-gallol and biotin-PEG(3400)-gallol leads to high particle stability under

physiological conditions. Particles could be freeze-dried and re-dispersed without noticeable corrosion or aggregation. Furthermore, they could be functionalized by the addition of a controlled number of neutravidin and biotinylated antibodies. Nanoparticles functionalized with human anti-VCAM-1 antibodies showed high binding affinity and specificity toward recombinant human VCAM-1 chimeras, whereas non-specific binding of neutravidin-coated nanoparticles was negligible, suggesting suitability for in vivo imaging of atherosclerosis. Importantly, any biotinylated ligand can be used to functionalize these MR contrast agents, which allows for targeting of any receptor that has a known ligand. Furthermore, comparison of immobilized ligand binding efficiencies can easily be accomplished by binding different biotinylated ligands to the neutravidin-decorated nanoparticles and performing in vitro binding studies. The particles can be produced with variable and controlled ligand densities. This and their ease to prepare and handle render them particularly well suited for research purposes. Finally, the family of catechol-derived anchors has been shown to strongly bind to a large variety of substrate types,^[47] in particular metal oxides. Thus, the surface modification concept presented in this work is a promising platform for the specific functionalization of a wide range of micro- and nanoparticle types.

5. Experimental Section

Materials: Biotin-PEG(3400)-NHS was purchased from Nektar, 3,4,5-Trihydroxyphenethylamine hydrochloride from Acros Organics, L- α -Phosphatidylcholine (egg-PC) and 1,2-Dipalmitoyl-*sn*-Glycero-3-Phosphoethanolamine-N-(Cap Biotinyl) (biotin-PE) from Avanti Polar Lipids, protein A, neutravidin, BSA and PBS (containing 2.67 mM KCl, 1.47 mM KH_2PO_4 , 137.93 mM NaCl and 8.5 mM Na_2HPO_4) from Invitrogen, Feridex from Berlex, human serum Percinorm U from Roche Systems, recombinant human VCAM-1 chimera and biotinylated human anti-E-selectin antibodies from R&D systems, biotinylated anti-human CD106 (VCAM-1) from Lubio science and all the other chemicals from Fluka. Fc-tagged human E-cadherin was a kind gift from Prof. Deborah E. Leckband.

Dispersant synthesis: mPEG(550)-gallol synthesized according to Studart et al.^[38] was a kind gift from André Studart. mPEG(5000)-gallol and biotin-PEG(3400)-gallol were synthesized following the same protocol as for mPEG-dopamine^[26] but using 6-hydroxy-dopamine instead of dopamine and mPEG(5000)-NHS respectively biotin-PEG(3400)-NHS. The average molecular weight of the dispersants was estimated based on matrix assisted laser desorption/ionization time of flight (MALDI-ToF) and nuclear magnetic resonance (NMR) spectra.

Particle synthesis: Iron oxide nanoparticles were synthesized by aqueous precipitation according to the protocol of Massart.^[24] Particles were neutralized by washing them with 10 mM 4-(2-hydroxyethyl)-1-piperazineethanesulfonic acid (HEPES) solution containing 150 mM NaCl. 24 μmol of PEG(550)-gallol or PEG(5000)-gallol dissolved in 25 mL Millipore water (18.2 M Ω) was added to a typical batch size resulting from 198.8 mg (1.2 mmol) FeCl_2 and

540.6 mg (2.3 mmol) FeCl_3 . Particles were dispersed in this solution by pulsed sonication (5 min, $P = 105 \text{ W cm}^{-2}$, pulse frequency = 1 s on, 1 s off, UP260s, Hirschler GmbH). To stabilize particles with a mixture of biotin-PEG(3400)-gallol and mPEG(550)-gallol, 25 mL Millipore-water containing 2.4 μmol of the former dispersant was added to uncoated particles before they were sonicated, followed by the addition of 21.6 μmol mPEG(550)-gallol. Particles were sonicated a second time according to the above described procedure. Excessive dispersants were removed by ultracentrifugation using a filter with a cut-off of 30 kDa (vivaspin, Epsom). The filter cake was re-suspended in Millipore water before the suspension was freeze-dried. Particles were re-suspended in PBS, HEPES, or Millipore water, sonicated for 30 min, and centrifuged for 10 min at 25 000 g (Eppendorf centrifuge 5417R) to eliminate agglomerates. The well-dispersed particles in the supernatant were collected and used for further studies.

Vesicle preparation: Egg-PC and biotin-PE were dissolved in chloroform. 0.5–2 wt% biotin-PE was added to egg-PC prior to drying this mixture to thin films under a steady flow of N_2 gas. The lipids were re-suspended in PBS at a concentration of 5 mg mL^{-1} . After allowing lipids to swell for 1 h, they were sonicated for 30 min using a bath sonicator (Aquasonic 75T, VWR Scientific products). Such-prepared vesicles were stored at 5 °C under N_2 for maximally 3 weeks.

Particle characterization: TEM imaging was performed on a Philips CM12 microscope operated at 100 kV and on a HRTEM Philips CM30 operated at 300 kV. Particles were suspended in Millipore-water at 60 $\mu\text{g mL}^{-1}$ before they were air-dried on 8-nm-thick carbon-coated 400-mesh Cu grids. Based on these TEM micrographs, the iron oxide core diameter was measured manually for 240 particles.

DLS experiments were conducted on a Brookhaven instrument 90 Plus particle size analyzer at a 90° angle using 100 $\mu\text{g mL}^{-1}$ PBS-based particle suspensions. Data were analyzed using a log normal fit. XDC experiments of 16 vol% HEPES-based particle suspensions were conducted on a BI-XDC machine (Brookhaven instruments limited) operated at 6000 rpm for 1 h. N_2 adsorption-desorption isotherms were measured at room temperature on a NOVA 1000 series Quantachrome machine. Before N_2 adsorption, freeze-dried, uncoated samples (NB. dried nanoparticles are respirable and thus potentially harmful) were degassed in vacuum at 160 °C for 2 h. The specific surface area was calculated using the Brunauer-Emmett-Teller method (BET).^[48]

Zeta potential: The zeta potential (DT-1200 dispersion technology, Inc.) was measured on 1 vol% Millipore water-based suspensions. These suspensions had previously been dialyzed against Millipore-water for 24 h. For titrations 1 M KOH and HNO_3 were used respectively.

Magnetic properties: SQUID measurements using vacuum-grease paste containing 0.03–3.17 wt% freeze-dried iron oxide nanoparticles were performed on a magnetic property measurement system at room temperature. The magnetization was calculated assuming the iron oxide core was Fe_3O_4 . A Bruker Avance 500 Wide Bore spectrometer (500 MHz for protons) fitted with a gradient amplifier (Bruker) for imaging using a fast spin-echo sequence in a 30-mm birdcage transmitter/receiver coil operated at 11.7 T was used for MRI. The slice thickness was 2 mm, field of view = 3.2 cm and the matrix = 64 \times 64 for T_1 and

T_2 -weighted images. For T_1 weighted images $T_E = 6.3$ ms, while T_2 -weighted images were performed using a Carr-Purcell-Meiboom-Gill sequence^[49] with $T_R = 3000$ ms and $T_\alpha = 10$ ms. MRI measurements were performed at 39°C. Relaxivities were calculated based on linear regressions through all data points shown in Figure 6b and c.

Dispersant quantification: The amount of adsorbed dispersant was quantified using TGA (TGA 500 Q series, TA Instruments) run from 25 to 400°C at a heating rate of 10°C min⁻¹ in N₂ atmosphere. Coupled to the TGA was an FTIR spectrometer (Thermo Nicolet Nexus 470 FT-IR) with which spectra of the volatile fractions coming off during TG analysis were measured every 30 s.

Neutravidin quantification: FACS experiments were conducted on a FACSCalibur instrument (BD Biosciences). FITC-labeled neutravidin was dissolved in PBS prior to the addition of 10 µg mL⁻¹ biotin-bearing particles. QCM-D studies^[50] were carried out on a Q-Sense E4 equipment (Q-Sense AB). Adding the PBS-based vesicle solutions in situ to SiO₂-coated quartz crystals (Q-Sense AB) resulted in the formation of biotinylated SLBs.^[51] Neutravidin was immobilized on the biotinylated SLBs prior to injection of biotinylated particles pre-coated with different amounts of neutravidin. The change in resonant frequency, Δf , and energy dissipation, ΔD , was measured in real time during the adsorption. The adsorbed mass can be approximated by $m = -17.7 \times \Delta f/n$ (ng cm⁻²) for the 5 MHz crystal used according to the Sauerbrey equation,^[52] where n is the overtone number.

QCM-D Binding Studies: 23 µg neutravidin was added to 500 µL HEPES containing 150 mM NaCl and 50 µg iron oxide nanoparticles stabilized with mPEG(550)-gallol and biotin-PEG(3400)-gallol (corresponding to 7 µmol neutravidin g_{iron oxide}⁻¹). Unless stated otherwise, 7.5 µg biotinylated anti-human VCAM-1 antibodies were added to neutravidin pre-coated particles. QCM-D studies were performed at room temperature in HEPES containing 150 mM NaCl (pH 7.4) under static conditions. A 400 ng cm⁻² protein A was adsorbed on SiO₂-coated QCM-D crystals from 50 µg mL⁻¹ solution followed by the addition of 5 µg mL⁻¹ recombinant human VCAM-1 chimera before 100 µg mL⁻¹ nanoparticles were injected. Between every step the system was rinsed with buffer. For control experiments, recombinant human VCAM-1 chimera was exchanged by Fc-tagged E-cadherins on the sensor substrate. Alternatively, biotinylated anti-human VCAM-1 antibodies were replaced by anti-human E-selectin antibodies on the nanoparticles. The mass concentrations were always kept constant. A concentration of 100 µg mL⁻¹ was used for the control experiment with BSA. Human serum was immobilised on Au-coated QCM-D crystals before functionalized particles, prepared according to the same procedure as described above, were injected into the QCM-D chamber.

Acknowledgements

The authors would like to thank Dr. Elisabeth Müller and Peter Tittmann (Electron Microscopy Center, ETH Zurich), Dr. André Studart (Nonmetallic Inorganic Materials, Department of

Material Science, ETH Zurich), Alkystis Phinikaridou and Prof. James A. Hamilton (Departments of Biophysics and Physiology and Biomedical Engineering, Boston University, MA), Viraj Tyagi (Boston University, MA), Prof. Dr. Bertram Batlogg (Department of Physics, ETH Zurich), and Prof. Deborah E. Leckband (Department of Chemical and Biomolecular Engineering, University of Illinois, IL) for their experimental support. COST action no. D43 "Multifunctional Superparamagnetic Iron Oxide Nanoparticles for Targeted Magnetic Resonance Imaging", ETH Zurich and the National Institutes of Health (NIH) are acknowledged for their financial support.

- [1] R. Weissleder, D. D. Stark, B. L. Engelstad, B. R. Bacon, C. C. Compton, D. L. White, P. Jacobs, J. Lewis, *Am. J. Roentgenol.* **1989**, 152, 167.
- [2] B. R. Bacon, D. D. Stark, C. H. Park, S. Saini, E. V. Groman, P. F. Hahn, C. C. Compton, J. T. Ferrucci, *J. Lab. Clin. Med.* **1987**, 110, 164.
- [3] M. Lewin, N. Carlesso, C. H. Tung, X. W. Tang, D. Cory, D. T. Scadden, R. Weissleder, *Nat. Biotechnol.* **2000**, 18, 410.
- [4] A. K. Gupta, M. Gupta, *Biomaterials* **2005**, 26, 3995.
- [5] S. Mornet, S. Vasseur, F. Grasset, P. Veverka, G. Goglio, A. Demourgues, J. Portier, E. Pollert, E. Duguet, *Prog. Solid State Chem.* **2006**, 34, 237.
- [6] A. E. Berkowitz, W. J. Schuele, P. J. Flanders, *J. Appl. Phys.* **1968**, 39, 1261.
- [7] D. L. Leslie-Pelecky, R. D. Rieke, *Chem. Mater.* **1996**, 8, 1770.
- [8] R. Weissleder, G. Elizondo, J. Wittenberg, A. S. Lee, L. Josephson, T. J. Brady, *Radiology* **1990**, 175, 494.
- [9] C. Chouly, D. Pouliquen, I. Lucet, J. J. Jeune, P. Jallet, *J. Microencapsul.* **1996**, 13, 245.
- [10] J. Kristian Raty, T. Liimatainen, M. Unelma Kaikkonen, O. Grohn, K. Jumani Airene, S. Yla-Herttuala, *Mol. Ther.* **2007**, 15, 2052.
- [11] F. A. Jaffer, R. Weissleder, *Circul. Res.* **2004**, 94, 433.
- [12] R. P. Choudhury, V. Fuster, Z. A. Fayad, *Nat. Rev. Drug Disc.* **2004**, 3, 913.
- [13] D. A. Sipkins, D. A. Cheres, M. R. Kazemi, L. M. Nevin, M. D. Bednarski, K. C. P. Li, *Nat. Med.* **1998**, 4, 623.
- [14] H. Pardoe, W. Chua-anusorn, T. G. St Pierre, J. Dobson, *J. Magn. Magn. Mater.* **2001**, 225, 41.
- [15] M. C. Bautista, O. Bomati-Miguel, X. Zhao, M. P. Morales, T. Gonzalez-Carreno, R. P. de Alejo, J. Ruiz-Cabello, S. Veintemillas-Verdaguer, *Nanotechnology* **2004**, 15, S154.
- [16] D. Hogemann, L. Josephson, R. Weissleder, J. P. Bacion, *Bioconjug. Chem.* **2000**, 11, 941.
- [17] C. J. Xu, K. M. Xu, H. W. Gu, R. K. Zheng, H. Liu, X. X. Zhang, Z. H. Guo, B. Xu, *J. Am. Chem. Soc.* **2004**, 126, 9938.
- [18] J. Xie, C. J. Xu, Z. C. Xu, Y. L. Hou, K. L. Young, S. X. Wang, N. Pourmond, S. H. Sun, *Chem. Mater.* **2006**, 18, 5401.
- [19] H. W. Gu, Z. M. Yang, J. H. Gao, C. K. Chang, B. Xu, *J. Am. Chem. Soc.* **2005**, 127, 34.
- [20] J. Xie, C. Xu, N. Kohler, Y. Hou, S. Sun, *Adv. Mater.* **2007**, 19, 3163.
- [21] K. Somaskandan, T. Veres, M. Niewczas, B. Simard, *N. J. Chem.* **2008**, 32, 201.
- [22] J. H. Gao, G. L. Liang, J. S. Cheung, Y. Pan, Y. Kuang, F. Zhao, B. Zhang, X. X. Zhang, E. X. Wu, B. Xu, *J. Am. Chem. Soc.* **2008**, 130, 11828.
- [23] H. W. Gu, K. M. Xu, Z. M. Yang, C. K. Chang, B. Xu, *Chem. Commun.* **2005**, 4270.
- [24] R. Massart, *IEEE Trans. Magn.* **1981**, 17, 1247.
- [25] Even though 6-hydroxy-dopamine is not a direct derivative of gallic acid because it has no acidic group on the phenol ring, we call it

- gallol for simplicity. It has three hydroxy groups directly linked to the phenol as is the case for gallic acid.
- [26] S. Zurcher, D. Wackerlin, Y. Bethuel, B. Malisova, M. Textor, S. Tosatti, K. Gademann, *J. Am. Chem. Soc.* **2006**, *128*, 1064.
- [27] S. C. Meyer, T. Gaj, I. Ghosh, *Chem. Biol. Drug Design* **2006**, *68*, 3.
- [28] M. I. Cybulsky, K. Iiyama, H. M. Li, S. N. Zhu, M. Chen, M. Iiyama, V. Davis, J. C. Gutierrez-Ramos, P. W. Connelly, D. S. Milstone, *J. Clin. Investig.* **2001**, *107*, 1255.
- [29] Y. Nakashima, E. W. Raines, A. S. Plump, J. L. Breslow, R. Ross, *Arterioscler. Thromb. Vasc. Biol.* **1998**, *18*, 842.
- [30] K. A. Kelly, J. R. Allport, A. Tsourkas, V. R. Shinde-Patil, L. Josephson, R. Weissleder, *Circul. Res.* **2005**, *96*, 327.
- [31] Y. X. J. Wang, S. M. Hussain, G. P. Krestin, *Eur. Radiol.* **2001**, *11*, 2319.
- [32] A. Barbieri, W. Weiss, M. A. Vanhove, G. A. Somorjai, *Surf. Sci.* **1994**, *302*, 259.
- [33] R. M. Cornell, U. Schwertmann, *The Iron Oxides*, Wiley-VCH, Weinheim, Germany 2003.
- [34] J. L. Dalsin, L. J. Lin, S. Tosatti, J. Voros, M. Textor, P. B. Messersmith, *Langmuir* **2005**, *21*, 640.
- [35] E. Taboada, E. Rodriguez, A. Roig, J. Oro, A. Roch, R. N. Muller, *Langmuir* **2007**, *23*, 4583.
- [36] S. Mornet, J. Portier, E. Duguet, *J. Magn. Magn. Mater.* **2005**, *293*, 127.
- [37] S. Yu, G. M. Chow, *J. Mater. Chem.* **2004**, *14*, 2781.
- [38] A. R. Studart, E. Amstad, L. J. Gauckler, *Langmuir* **2007**, *23*, 1081.
- [39] F. Q. Hu, L. Wei, Z. Zhou, Y. L. Ran, Z. Li, M. Y. Gao, *Adv. Mater.* **2006**, *18*, 2553.
- [40] A. K. Gupta, S. Wells, *IEEE Trans. Nanobiosci.* **2004**, *3*, 66.
- [41] J. Vidal-Vidal, J. Rivas, M. A. Lopez-Quintela, *Colloids Surf. A Physicochem. Eng. Asp.* **2006**, *288*, 44.
- [42] J. Hong, D. M. Xu, J. H. Yu, P. J. Gong, H. J. Ma, S. D. Yao, *Nanotechnology* **2007**, *18*.
- [43] S. A. Darst, M. Ahlers, P. H. Meller, E. W. Kubalek, R. Blankenburg, H. O. Ribi, H. Ringsdorf, R. D. Kornberg, *Biophys. J.* **1991**, *59*, 387.
- [44] S. R. Wan, J. S. Huang, M. Guo, H. K. Zhang, Y. J. Cao, H. S. Yan, K. L. Liu, *J. Biomed. Mater. Res. A* **2007**, *80A*, 946.
- [45] M. D. Shultz, J. U. Reveles, S. N. Khanna, E. E. Carpenter, *J. Am. Chem. Soc.* **2007**, *129*, 2482.
- [46] J. Stohr, *NEXAFS Spectroscopy*, Springer-Verlag, **1992**.
- [47] H. Lee, S. M. Dellatore, W. M. Miller, P. B. Messersmith, *Science* **2007**, *318*, 426.
- [48] S. Brunauer, P. H. Emmett, E. Teller, *J. Am. Chem. Soc.* **1938**, *60*, 309.
- [49] S. Meiboom, D. Gill, *Rev. Sci. Instrum.* **1958**, *29*, 688.
- [50] M. Rodahl, F. Hook, A. Krozer, P. Brzezinski, B. Kasemo, *Rev. Sci. Instrum.* **1995**, *66*, 3924.
- [51] C. A. Keller, B. Kasemo, *Biophys. J.* **1998**, *75*, 1397.
- [52] G. Sauerbrey, *Zeitschrift Fur Physik* **1959**, *155*, 206.

Received: September 11, 2008
Revised: November 30, 2008
Published online: February 25, 2009